

Modeling the Evolution of Terrestrial and Water-rich Planets and Moons

Lena Noack, Attilio Rivoldini, Tim Van Hoolst

Department of Reference Systems and Planetology
Royal Observatory of Belgium (ROB)
Brussels, Belgium

Email: lena.noack@oma.be, attilio.rivoldini@oma.be, tim.vanhoolst@oma.be

Abstract—We completed the numerical code CHIC (short for *Coupling Habitability, Interior, and Crust*) for thermo-chemical simulations of the evolution of both terrestrial and water-rich planets and moons. The study focusses on the numerical aspects of the code implementations and their validation. The thermal evolution of the mantle is calculated either by solving the energy conservation equation supplemented by boundary-layer theory (1D parameterized thermal evolution model) or by solving the energy, mass, and momentum conservation equations (2D/3D convective thermal evolution). For the latter setting, the equations can be solved in both incompressible and compressible formulations and can include chemical buoyancy effects for an inhomogeneous mantle by applying a particles-in-cell method. The code provides a user updatable library of thermodynamic properties of core, mantle and water/ice materials derived from the associated equations of state. CHIC has been benchmarked with different convection codes, and has been compared to published interior-structure models and 1D parameterized models. CHIC is an advanced simulation code that can be applied to a diverse range of geodynamic problems and questions.

Keywords—fluid dynamics; convection; numerical modeling; thermal evolution; planetology.

I. INTRODUCTION

To understand geophysical processes in a planet like Earth including convection, surface processes as plate tectonics or volcanism, and the evolution of mantle and atmosphere, numerical models are essential tools [1] and have been applied in the past decades to investigate various planets and moons. Numerical simulations are especially needed for the investigation of feedback cycles between the interior and the surface, as, for example, the CO₂-cycle (where subduction of carbonates helps to regulate surface temperatures over geophysical timescales), the subduction cycle (delivering volatiles to the mantle and releasing volatiles by volcanic outgassing), the evolution of continents (stabilizing plate tectonics) and the possible maintenance of a magnetic field by strong cooling of the core. These processes are likely important for the habitability of Earth, i.e., for the ability to host life, and may also play an important role for other planets [2], [3].

Different numerical models have been applied to study the evolution of terrestrial planets or moons in the literature, either focussing on the mantle convection pattern in 2D or 3D geometries, or investigating the general thermal evolution with 1D parameterized models.

In this study, we couple both methods in one simulation code CHIC together with a library of thermodynamic properties that can be applied to self-consistently determine the interior structure of a planet and its later evolution depending on key factors as, for example, the planet mass, composition, and initial temperature profile.

The paper is organized as follows: Section II gives an overview of the state of the art and the progress in numerical modelling via the CHIC code. In Section III, we describe the different modules of CHIC, followed by the validation of the correctness of the models in Section IV. Finally, in Section V, we summarize the possibilities of a coupled 1D - 2D/3D code and the planned future work.

II. STATE OF THE ART

Several 2D and 3D convection codes have been developed over the past decades to investigate Earth-like planets. They typically concentrate solely on either the thermal evolution or do steady-state snapshots of the mantle and crust. Some models include the simplified evolution of the core [4] or of the atmosphere [5], [6] as boundary conditions to the mantle convection simulation. In such a convection model, lateral variations in the mantle can be investigated, including mantle plumes, local melt regions, and plate motions.

On the other hand, a 1D model assumes a laterally averaged profile for temperature and material properties. As a result, simulations of, for example, the volcanic history of a terrestrial planet may differ between 1D and 2D/3D models.

1D thermal evolution models also have several advantages over 2D/3D convection models. Parameterization models [7] are applicable over a large parameter space (applicable also at high convection velocities, where convection models suffer from numerical problems), and include the simulation of both liquid and solid materials. Especially, strongly convecting systems (e.g., liquid core or ocean) can be simulated, which is generally infeasible for planetary convection codes, as they will either produce numerical instabilities or require an unacceptably large amount of computational power. 1D models are very fast compared to convection models. Depending on the specific application, a 1D thermal evolution model runs in the order of seconds or minutes, whereas 2D/3D models (that typically need a high resolution to avoid numerical errors) may run for days or weeks.

To understand different geophysical processes and feedback cycles on Earth-like or water-rich planets, a coupled model

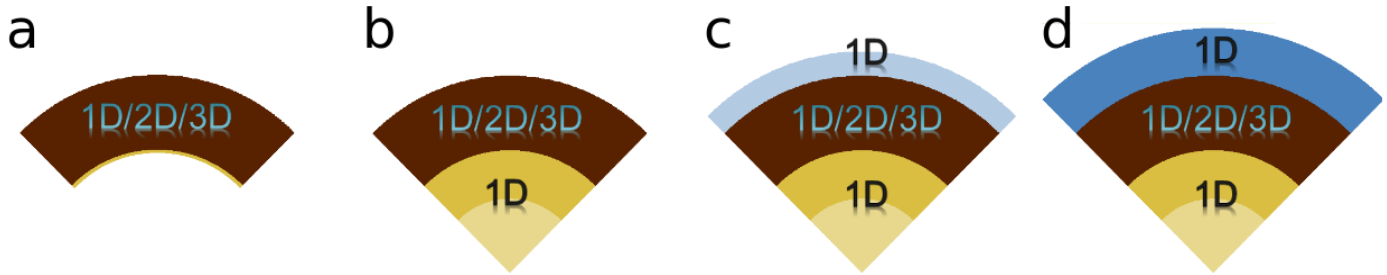


Figure 1. Possible configurations that are investigated with CHIC: a) mantle with variable CMB temperature, b) mantle with core evolution and inner core freezing, c) mantle and core with an atmosphere, d) mantle and core with a deep ocean on top (we neglect here a possible atmosphere).

is needed that can combine 1D parameterized models (for example for the treatment of the water-layer or the core) with 2D mantle convection models.

We therefore developed a new code CHIC at the Royal Observatory of Belgium, that combines different numerical models in one toolbox. The code is written in Fortran, which allows for fast simulations (either running on one processor or in parallel) on standard high-performance clusters.

The CHIC code is able to treat both 1D parameterized models (using the thermal boundary layer theory to determine the temperature evolution in a terrestrial planet [7], [8] or ocean planet [9]) and 2D/3D models to investigate the detailed convection pattern in a silicate mantle or ice layer over time.

In our implementation, the planets are assumed to consist of several different spherical layers (shells). The lowermost shell represents the core and is overlain by a silicate shell (mantle and crust) and a potential water-ice layer. The uppermost shell represents the planets atmosphere. All shells are thermally coupled, i.e., the heat flux and temperature are continuous at each interface between the different layers. The surface temperature is allowed to vary with time depending on the greenhouse gases in the atmosphere, or is taken constant if changes in the atmosphere are neglected.

CHIC allows the user to apply different 1D or 2D/3D modules as needed: for the core, either only changes in the core-mantle boundary (CMB) temperature are investigated, or a 1D parameterized model of the iron core including inner core freezing is applied (Figures 1(a) and 1(b)); the thermal state of the mantle and high-pressure ice layers are investigated either via a convection model or a 1D parameterized model; the atmosphere and a potential water ocean (Figures 1(c) and 1(d)) are investigated with a 1D module, whereas ice layers could be investigated also with the 2D/3D convection module. CHIC is therefore a powerful tool for the investigation of the evolution of terrestrial or ocean planets - from interior to atmosphere - and their possible habitability.

III. MODELS

CHIC uses various modules for modelling different shells of a terrestrial or ocean planet. The basic modules provided by CHIC are listed below. The density of the material and

other physical properties are determined as described in Section III-A, and can be applied to both 1D and 2D/3D modules. The input file used for the simulations is similar for all modules, which simplifies comparison of the 1D model with the 2D mantle model.

A. Interior structure model and material properties

Within CHIC, simple interior structure models can be generated to assess the radius of a terrestrial planet for given mass, composition, and temperature profile. Those models assume a spherical planet that is differentiated into an iron core, a silicate shell, and an optional ocean layer. For the silicate mantle we assume an Mg-end member olivine system. We neglect high pressure olivine polymorphs but allow for the disassociation of olivine to perovskite and Mg-wstite and the occurrence of post-perovskite at high pressure and temperature. Material properties (density ρ , thermal expansion coefficient α and heat capacity c_p) are computed from equations of state for variable pressure and temperature [10], [11].

The gravitational acceleration $g(r)$ as a function of radius r is determined from the Poisson equation, it depends on the gravity value at the surface of the planet,

$$dg/dr = 4\pi G \rho - 2g/r \quad (1)$$

where G is the gravitational constant.

The pressure as a function of depth is calculated by assuming hydrostatic equilibrium and depends on the atmospheric pressure at the surface:

$$dp/dr = -g\rho \quad (2)$$

The mass $m(r)$ is

$$dm/dr = 4\pi r^2 \rho \quad (3)$$

B. Core evolution model

The 1D core evolution module determines the variation of upper core temperature with time via the energy conservation equation

$$\rho_c c_{p,c} V_c \varepsilon_c dT_c/dt = -q_c A_c \quad (4)$$

where the index c denotes core values, V_c is the core volume and A_c the core surface area, ε_c is a constant relating the average core temperature to the CMB temperature, t is the time and q_c is the heat flux from the core into the mantle (defined via the heat flux that the mantle can take up, e.g., [8]),

$$q_c = -k_m dT/dr|_{r=R_c} \quad (5)$$

where k_m is the mantle thermal conductivity. We neglect radioactive heat sources in the core, as well as tidal heating effects. If the freezing of an inner core is considered, additional terms for latent heat and gravitational energy release have to be added in Eq. (4) [12]. For 2D/3D convection models, temperature is calculated at pre-defined grid points, and the average temperature gradient at the CMB is calculated over the two bottom shells of the mantle grid; in the 1D parameterized model, the heat flux is computed from the boundary-layer theory.

For the thermal evolution, either a pure iron core or an iron-rich core containing lighter elements like sulfur is considered. In the latter case, core freezing can be modelled if the core temperature falls below the melting temperature. This model, however, only works if the freezing of the core starts at the core center (leading to a solid inner core as on Earth). This may not be the case for Mercury or Ganymede, where iron may solidify in the upper part of the core and sink down as (so-called) iron snow.

We only model planets without the iron snow regime and adopt the model of [4], which determines latent heat released by iron solidification and gravitational energy produced by differentiation of the core into an inner and outer core. Both mechanisms have an influence on the thermal evolution of the mantle. For super-Earths (i.e., planets up to 10 Earth masses), we neglect lighter elements in the core, as material properties for those are only known for a limited pressure range.

C. Mantle: 1D parameterized model

The 1D module assesses the thermal evolution of the mantle based on [7], [8], [9]. We refer to these references for full details. The model determines the evolution of the upper mantle temperature T_m over time by considering that the loss of energy due to mantle cooling and heat flux out of the mantle is balanced by the heat flux from the core into the mantle and the radioactive heat production in the mantle (we neglect heat produced by tidal friction):

$$\varrho_m c_{p,m} V_l \varepsilon_m dT_m/dt = -q_l A_l + q_c A_c + Q_m V_l \quad (6)$$

The index m denotes mantle values. V_l is the volume of the mantle from core to the base of the lithosphere, and A_l is the area at the boundary between mantle and lithosphere. The constant ε_m relates the average mantle temperature with T_m . The mantle temperature decreases due to heat flux out of the mantle into the lithosphere q_l , increases due to inflowing heat flux from the core q_c and increases with heat released by radioactive heat sources Q_m .

CHIC also allows to model possible melting events and crust formation over time. This leads to additional terms in (6). For details on the crustal evolution, as well as the definition of the thermal boundary layers and calculation of the temperature in the lithosphere, we refer to [8]. Note that the 1D parameterized model only considers the evolution of the temperature over time, and assumes effective convection. To understand the convection mechanism and its strength depending on mantle parameters and planet size (possibly triggering plate tectonics at the surface), a more sophisticated 2D/3D convection model is needed.

D. Mantle: 2D / 3D convection model

The CHIC code uses a finite volume (FV) field approach to solve the conservation equations of mass, momentum and energy. A finite grid is placed in the mantle, with shells from the CMB to the planet surface, and a predefined number of grid points per shell. We then define Voronoi cell volumes around each grid point and solve the system of equations on each cell volume considering the flux in and out of the cell and the energy production in the cell. We employ a staggered grid, see Figure 2, where the scalar values like temperature (T) and pressure (p) are defined at the cell center (i,k), whereas the lateral and radial velocities u, w are defined at the cell faces. The viscosity η is calculated at the cell centers (CV) and is interpolated at the cell nodes (N) and cell faces (A,B,C in x-,y- and z-direction) with a geometric averaging scheme.

The grid is either defined in Cartesian coordinates in a 2D or 3D box or in polar coordinates for a 2D cylindrical sphere (a cut through the planet at the equator representing the temperature profile of a cylinder with the 2D plane as a basis) or a 2D spherical annulus (an equatorial cut or polar section that approximates the temperature profile of a sphere in 3D, [13]), see Figure 3. For the 2D models with spherical or cylindrical geometry, it is often useful to employ a regional sector of the 2D spherical model (as shown in Figure 6). In addition to the grid, randomly distributed particles (also called tracers) are used to transport local information as for example density variations or water content, see Section III-D3.

In CHIC, the thermal (or thermochemical, see Section III-D3) evolution can be modelled either for an incompressible medium with the Boussinesq approximation (BA) or the Extended-Boussinesq approximation (EBA), or for a compressible medium with the (truncated) anelastic liquid approximation (TALA/ALA).

1) *(Extended) Boussinesq approximation:* We solve the equation system for an incompressible medium either with the Boussinesq approximation (BA), which neglects the influence of compressibility on the mantle, or we apply the Extended-Boussinesq approximation (EBA), which yields an adiabatic temperature increase with depth depending on the dissipation number $Di = \alpha g D / C_p$, where D is the mantle thickness (see [7] for details on the model). For a dissipation number Di of zero, the formulation reduces to the Boussinesq approximation (BA). We therefore concentrate on the EBA model below.

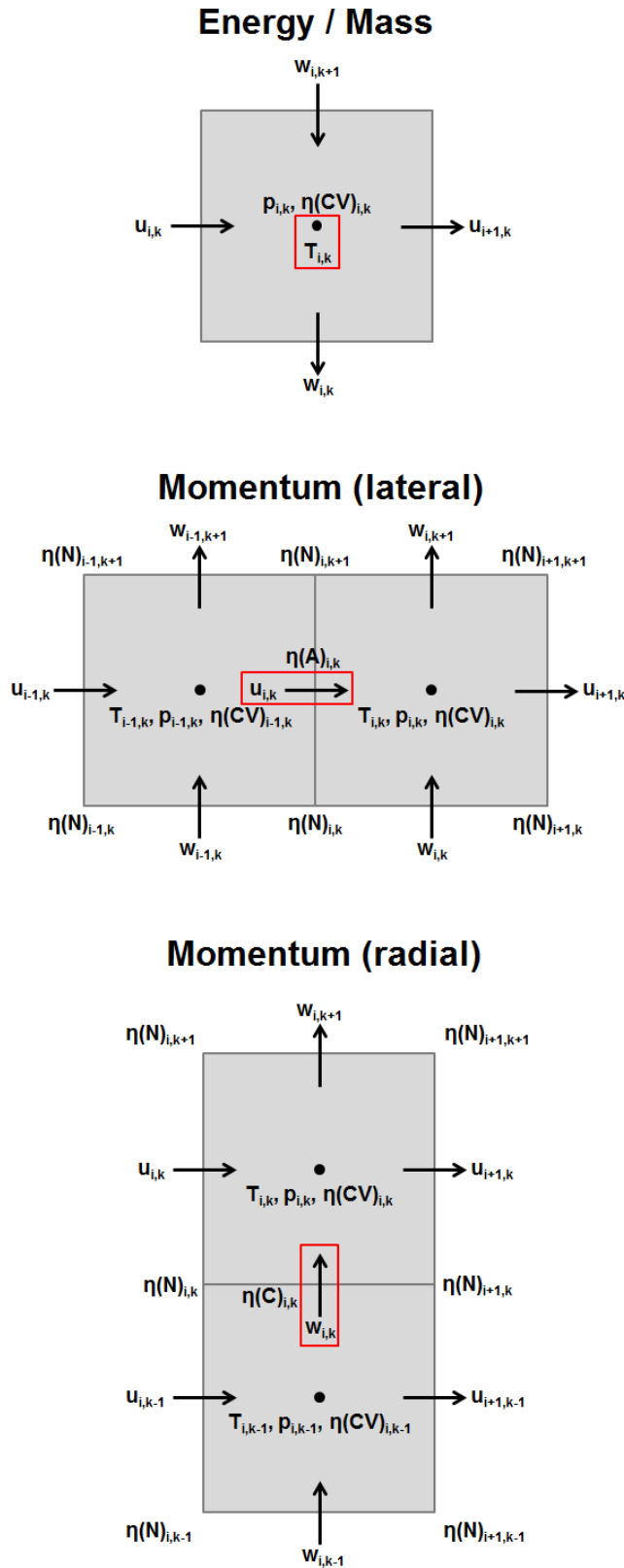


Figure 2. The staggered grid enforces different local solver meshes for the energy, mass and momentum conservation equations. The center of each local mesh is highlighted with a red box.

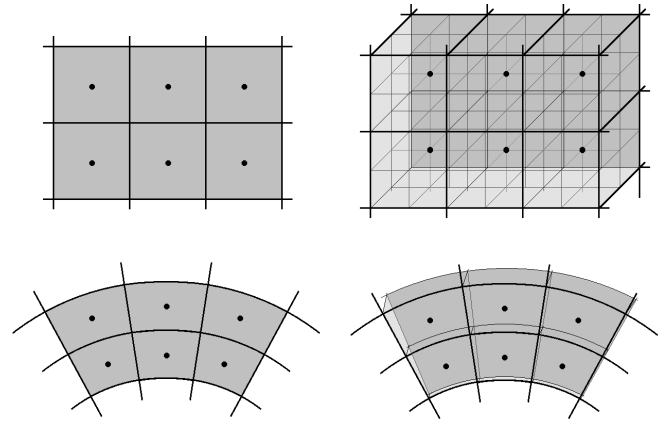


Figure 3. Geometries implemented in CHIC. Top: 2D Cartesian box and 3D Cartesian box. Bottom: 2D cylinder and 2D spherical annulus.

In the EBA approximation, the non-dimensional conservation equations of energy, mass and momentum can be expressed as (e.g., [14]):

$$\frac{\partial T}{\partial t} + \vec{v} \cdot \nabla T + Di(T + T_0)\vec{v}_r = \nabla^2 T + \frac{Di}{Ra}\Phi + H \quad (7)$$

$$\nabla \cdot \vec{v} = 0 \quad (8)$$

$$-\nabla p + \nabla \cdot \sigma = RaTe_r \quad (9)$$

$$\sigma = \eta \left(\nabla \vec{v} + \nabla \vec{v}^T \right) \quad (10)$$

Here, T is temperature, T_0 surface temperature, t time, and Di the dissipation number. The convective pressure is denoted by p ; \vec{v} is the velocity and \vec{v}_r the radial velocity, whereas e_r is the radial unit vector. H is the heat source (e.g., radioactive heat source). σ the convective stress tensor, η is the viscosity, and \top indicates a transposed matrix. The Rayleigh number Ra is a measure for the convective vigour

$$Ra = \frac{\rho g \alpha D^3 \Delta T}{\kappa \eta_{ref}} \quad (11)$$

where ΔT is the mantle temperature contrast, $\kappa = k/(\rho C_p)$ the thermal diffusivity and η_{ref} a reference viscosity defined at a reference temperature, pressure and stress (for non-Newtonian viscosity), see Section III-D5. Φ is the viscous dissipation [7], [13], [14]

$$\Phi = \frac{1}{2} \sigma : \dot{\epsilon} = \eta \dot{\epsilon} : \dot{\epsilon} \quad (12)$$

with strain rate tensor $\dot{\epsilon} = \partial v_i / \partial x_j$.

Equations (7)-(9) are written in a non-dimensional form [15]. The non-dimensionalization is obtained by dividing the dimensional value of each variable by a reference value as given in [15]. The quantities given in Section IV are also non-dimensional values.

2) *Anelastic liquid approximation*: While the (Extended) Boussinesq approximation models a constant density in the mantle, in reality the density increases with depth due to pressure-induced compression. In Mars' and Mercury's mantle the compressibility effect is small and is typically neglected. For Earth-size and larger planets the density increases significantly within the mantle and is typically addressed in mantle convection codes via the (truncated) anelastic liquid approximation (short TALA or ALA), see [7] and [14].

Reference profiles are employed for the pressure, density and temperature ($\bar{p}, \bar{\rho}, \bar{T}$), as well as lateral variation fields due to convection (p', ρ', T'):

$$\begin{aligned} T &= \bar{T} + T' \\ p &= \bar{p} + p' \\ \rho &= \bar{\rho} + \rho' \end{aligned}$$

In addition, we apply reference profiles for the gravitational acceleration, thermal expansion coefficient, heat capacity at constant volume or pressure, bulk modulus and Grüneisen parameter ($\bar{g}, \bar{\alpha}, \bar{C}_v, \bar{C}_p, \bar{K}_T, \bar{\gamma}$).

The conservation equations of mass and momentum for the ALA formulation are solved together in a coupled system and read in non-dimensional quantities [7]

$$\nabla \cdot (\bar{\rho} \vec{v}) = 0 \quad (13)$$

$$-\nabla p' + \nabla \cdot \sigma + Di \frac{\bar{\rho} \bar{g} p' C_p}{\bar{\gamma} \bar{K}_T C_v} \vec{e}_r = Ra \bar{\rho} \bar{g} \bar{\alpha} (T - \bar{T}) \vec{e}_r \quad (14)$$

$$\sigma = \eta \left(\nabla \vec{v} + \nabla \vec{v}^T - \frac{2}{3} \nabla \cdot \vec{v} I \right) \quad (15)$$

I is the identity tensor. C_p and C_v are the specific heat at constant pressure and volume, K_T is the isothermal bulk modulus.

In the truncated anelastic liquid approximation (TALA), the third term in equation (14) is neglected

$$-\nabla p' + \nabla \cdot \sigma = Ra \bar{\rho} \bar{g} \bar{\alpha} (T - \bar{T}) \vec{e}_r \quad (16)$$

The TALA formulation is a simplified compressible formulation that is favoured by several codes to avoid numerical problems due to the additional ALA term (third term in Eq. (14)). Furthermore, this term is often neglected as it requires knowledge of several material properties (as Grüneisen parameter or isothermal bulk modulus) depending on pressure, which requires the usage of an equation of state.

The energy conservation equation for the composite temperature field ($T = \bar{T} + T'$) can be expressed as

$$\begin{aligned} \bar{\rho} \bar{C}_p \left(\frac{\partial T}{\partial t} + \vec{v} \cdot \nabla T \right) &= \nabla \cdot (\bar{k} \nabla T) + Di \bar{\alpha} \bar{\rho} \bar{g} v_r (T + T_0) \\ &+ \frac{Di}{Ra} \Phi + \bar{\rho} H. \end{aligned} \quad (17)$$

3) *Thermochemical formulation*: Chemical inhomogeneities influence the convective behaviour. Buoyancy results from both thermal and compositional variations. The buoyancy term in Equation (9) changes to

$$Ra [(T - \bar{T}) - B (1 - d)] \vec{e}_r \quad (18)$$

for the BA and EBA formulation, for the TALA and ALA formulation it changes to

$$Ra \bar{\rho} \bar{g} [\bar{\alpha} (T - \bar{T}) - B (1 - d)] \vec{e}_r, \quad (19)$$

where B is the buoyancy number defined here as $1/(C_{p,0} \alpha_0)$ and $d = C_{ref} - C$ is the nondimensional density variation (a value of 0 denotes reference mantle material density C_{ref} and a positive d value a decreased local density). Such a chemical density variation can occur for example from partial melting or subduction of crustal material. Note that the chemical density variation is different from the compressible density increase with depth. The conservation of the chemical field C is modelled similarly to the energy conservation

$$\frac{\partial C}{\partial t} + \vec{v} \cdot \nabla C = \frac{1}{Le} \nabla^2 C \quad (20)$$

where Le is the Lewis number, which is a dimensional number defined as the ratio of thermal diffusivity κ to chemical diffusivity κ_c . For rocks, the chemical diffusivity is negligibly small and often set to zero. However, solving Eq. (20) without the diffusion term leads to numerical problems. In convection codes therefore either large Lewis numbers are used, or the particle are used instead of a chemical field to trace local density variations. In that approach, the particles are advected along the convective stream lines at the end of each time step via a Runge-Kutta method of fourth order. Averaged cell values are obtained by arithmetic averaging of particle values of all particles in the cell weighted by the reciprocal distance of the particle to the cell centre.

4) *Solver routines*: The energy equation is solved with a second-order implicit Euler method. To solve the conservation equation of mass and momentum, we either use a direct solver or a coupled mass and momentum solver. The direct solver uses one solver matrix for (8) and (9) and applies a penalty formulation following [16]. The iterative, coupled solver employs a pressure correction algorithm called SIMPLER following [16], [17]. In this paper, we apply the direct solver.

The resulting linear equations (for mass, momentum and energy) are solved iteratively with either the Pardiso solver [18] or a biconjugate gradient (BiCG) solver with an under-relaxation scheme. The BiCG solver is slower compared to the Pardiso solver, but is advantageous for parallelization in combination with the SIMPLER pressure correction.

5) *Viscosity formulations*: The equations above depend on the viscosity of the material η . The viscosity depends on several factors including the temperature, pressure, grain size, water content and strain rate of a material. In the mantle of the Earth, creep is typically described by dislocation creep (motion of dislocations through the crystal lattice) and diffusion creep (deformation of crystalline solids by the diffusion of vacancies through their crystal lattice). The latter is largely independent

of the strain-rate, whereas dislocation creep does not depend on the grain size. In CHIC, the user can choose between a dislocation viscosity, a diffusion viscosity and a mix of both formulations. The smaller viscosity is the dominant viscosity for material motion.

The general equation used in CHIC for the viscosity follows an Arrhenius law [19], [20]

$$\eta = A \dot{\epsilon}_{II}^{\frac{1-n}{n}} d^{\frac{p}{n}} C_{OH}^{\frac{-r}{n}} \exp\left(\frac{E + pV}{nRT}\right) \quad (21)$$

A is a material-dependent constant, n is the stress exponent, d is the grain size, C_{OH} is the concentration of water (for dry materials $r=0$), r is the water exponent, E the activation energy and V the activation volume. p is the pressure and R the gas constant. Note that the pressure p is the hydrostatic pressure and not the convective pressure as in (9). The parameters for both diffusion and dislocation creep are taken from [19], [20] for both wet and dry materials. The concentration of water C_{OH} is traced via particles and does not only influence the viscosity, but also the local melt temperature, which is smaller in the presence of water than for dry materials [21].

Even though the Arrhenius viscosity (21) is preferentially used for simulations of terrestrial planets, for benchmarks and basic convection simulations typically an approximated viscosity is used, the so-called Frank-Kamenetskii approximation (FKA), given by

$$\eta = A \exp(-\theta_T T + \theta_p z) \quad (22)$$

Here, θ_T and θ_p are either the logarithm of a pre-defined viscosity contrast with respect to temperature or pressure, respectively, or they are derived from the parameters in (21) [22]. z is the non-dimensional depth (0 at the surface and 1 at the CMB). Note that for the application to plate tectonics simulations, the FKA (22) may not be suitable as shown in [22] and the Arrhenius viscosity (21) should be applied.

E. OpenMP and MPI parallelisation

The Pardiso solver [18], that can be used to solve the linear equations for the mass-momentum and energy equations (see Section III-D4), can employ an automatic OpenMP parallelization. In addition, we implemented an MPI domain decomposition for the mesh. The domain is separated into several subdomains, on which the conservation equations of mass, momentum and energy are solved individually. However, the solution on each subdomain depends on the neighbouring domains. For this reason, additional boundary cells (ghost cells) are added at the boundary between subdomains, which contain the corresponding values (for example, temperature or velocity) from the neighbour domain and serve as boundary cells for their respective MPI domain. After the equation system is solved, ghost cells are updated with the new values from their neighbour domain and the conservation equations are re-solved. This iteration continues until convergence occurs for the root-mean-square velocity.

Figure 4 shows the domain decomposition for four CPUs using either non-periodic or periodic boundary conditions

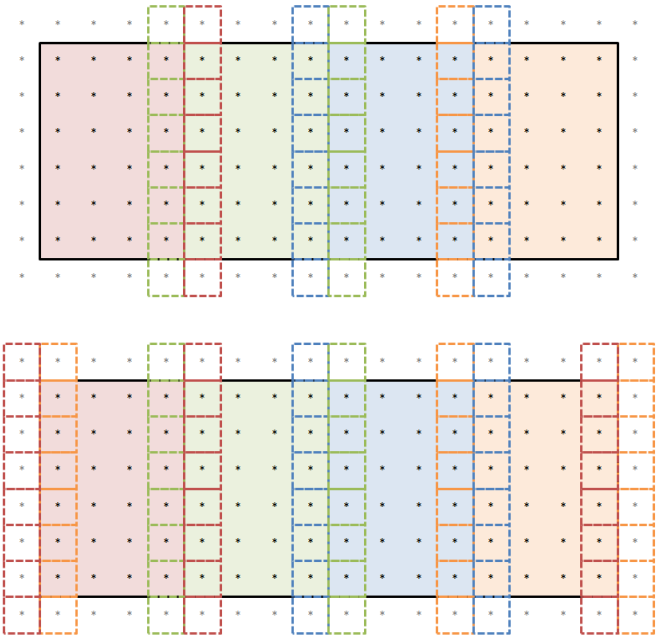


Figure 4. Schematic mesh decomposition for a 2D Cartesian box using four CPUs. Additional cells at the domain boundaries are highlighted in the respective domain color. The upper plot uses a free-slip, reflective side boundary condition, the lower plot applies a periodic boundary condition.

at the left and right side of the box. The bottom and top boundaries are free-slip boundaries (the temperature values are either pre-set boundary values or evolve over time at the 1D model interface for core or ocean/atmosphere). Grey stars denote boundary cells, boxes with coloured boundaries are ghost cells, and black dots denote the cells, for which the mass, momentum and energy equations are solved.

The MPI speed-up factor and simulation times are plotted in Fig. 5 for different grid sizes (shells) and amounts of CPU for a 2D Cartesian box and aspect ratio 1 (i.e., same number of grid points in lateral directions as number of shells) for the first 10 time steps, where the simulation parameters are taken from the first benchmark case in Blankenbach et al. [23]. Here, the Pardiso solver is applied (see Section III-D4). The high-performance SGI cluster, on which the simulations were executed, contains nodes with 24 CPU cores and two Xeon E5-2680V3 processors per node.

The speed-up factor is based on simulations with two CPUs instead of one. The update of the ghost cells (boxes with coloured boundary in Fig. 4) demands at least two iterations to solve the coupled mass-momentum equation system. When using only one CPU, no update of ghost cells and thus no additional iteration is needed. The parallel version can therefore never show a perfect speed-up behaviour when using one CPU as reference. The effect of parallelization on the simulation time can also be observed in the right plot in Fig. 5.

For small grid sizes with 20, 40 or 80 shells, the speed-up

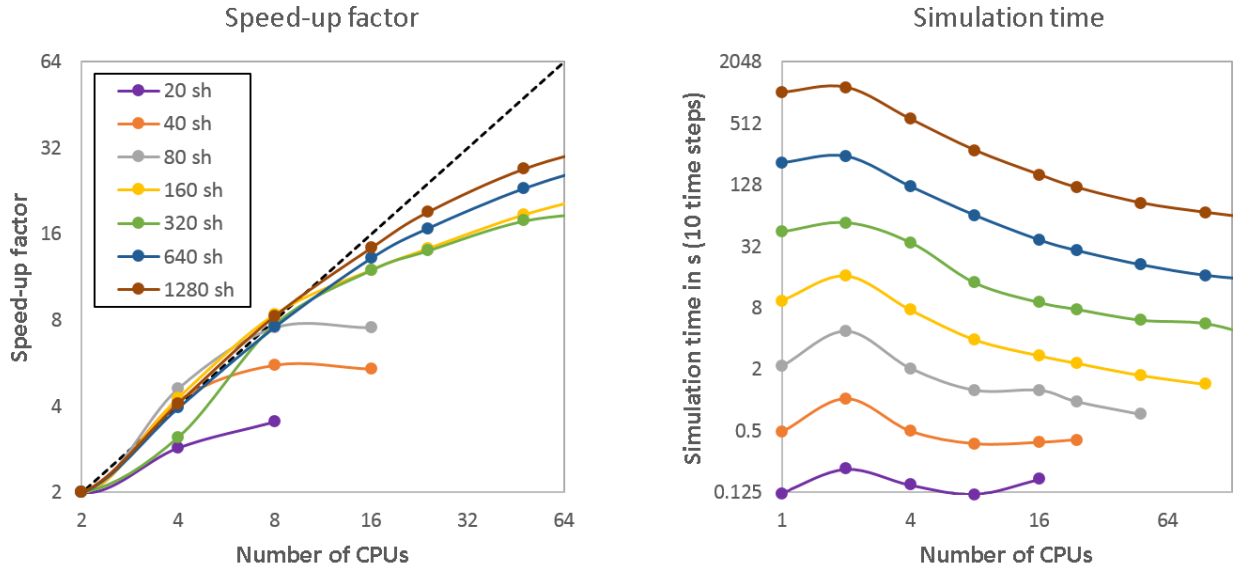


Figure 5. Left: scaling factor for MPI parallelization using different grid sizes (20sh stands for 20x20 grid points plus boundary cells) based on a reference time obtained for 2CPUs. Right: simulation time in seconds for different amounts of CPU for the same simulations.

factor decreases to non-optimal behaviour (i.e., curve drops below the black dotted line) when using more than 2, 4 and 8 CPUs, respectively. For larger grids the simulations show an optimal speed-up behaviour up to approximately 24 CPUs, which is the number of CPUs per node on the used HPC architecture. The simulation time is still steadily reduced with increasing number of CPUs.

When employing a larger 2D grid size with doubled resolution, the number of grid points is four times larger. The right plot in Fig. 5 shows that the simulation time also increases by a factor ~ 4 for doubled resolution.

IV. CODE VALIDATION RESULTS

In this section, we present several benchmark tests that have been applied to validate the code.

A. Incompressible model

To validate our 2D Cartesian box implementation of the thermal convection simulation in the incompressible approximation we compare it to the standard benchmark by Blankenbach [23]. The benchmark assumes either isoviscous convection or temperature- and pressure-dependent viscosity in the Boussinesq approximation. A free-slip boundary condition is applied to the walls of the box. The non-dimensional temperature at the surface of the box is set to 0 and at the bottom to 1. The simulations are run until steady-state is reached (i.e., variations of the non-dimensional temperature drop below a tolerance value of 10^{-10}).

In Table I, we compare our results (for a fixed resolution of 80(200)x80 cells for aspect ratio 1 or 2.5) to the published

TABLE I. BENCHMARK COMPARISON OF CHIC (CH) TO [23] (BL).

	RMS velocity		Max temperature		Nusselt number	
	CH	BL	CH	BL	CH	BL
1a	42.92	42.74-42.87	0.425	0.421-0.427	4.920	4.864-4.896
1b	194.3	192.4-198.0	0.432	0.415-0.437	10.60	10.42-10.69
1c	835.1	823.7-842.5	0.440	0.431-0.446	21.81	21.08-22.07
2a	496.6	458.3-503.3	0.725	0.716-0.741	10.43	10.04-10.07
2b	183.1	166.7-193.1	0.390	0.385-0.403	7.271	6.806-7.409

Case 1: isoviscous material, $\ell=1$, a) $Ra=1e4$, b) $Ra=1e5$, c) $Ra=1e6$.

Case 2: FKA (11), a) $Rasurf=1e4$, $\theta_T=\ln(1000)$, $\theta_p=0$, $\ell=1$,
b) $Rasurf=1e4$, $\theta_T=\ln(16384)$, $\theta_p=\ln(64)$, $\ell=2.5$.

results. Note that in [23] different resolutions have been used, therefore we give the min and max values for resolutions of at least 33x33 cells. Here, we provide only the three most important quantities: the root-mean-square (RMS) velocity, the maximum of the upper mantle temperature profile at the middle of the box (0.5ℓ , where ℓ is the length divided by height, i.e., the aspect ratio) and the surface Nusselt number, which is a measure of the ratio of convective to conductive heat transport at the surface of the box. For more information on the benchmark setup we refer the reader to [23]. CHIC yields results that are in good agreement with all cases published in [23], see Table I. They are either within the range of published results or differ by less than 4%.

A comparison between different geometries (Cartesian box in two or three dimensions, 2D cylindrical shell and 3D sphere) for the Boussinesq approximation has been published by Noack and Tosi [24] using the convection code GAIA [25]. To verify our implementation of the different geometries, we compare the CHIC code to the published results with respect to RMS velocity, average mantle temperature and surface Nusselt number. For the 2D box, we apply a resolution of

TABLE II. BENCHMARK COMPARISON OF CHIC (CH) TO [24] (NT)

Case	RMS velocity		Average temperature		Surface Nusselt number	
	CH	NT	CH	NT	CH	NT
2D box, $\ell=1$, RBC ^a	54.59	53.81	0.689	0.6872	1.987	1.956
2D box, $\ell=2$, RBC ^a	54.59	53.79	0.689	0.6871	1.987	1.956
2D box, $\ell=1$, PBC ^b	55.61	54.62	0.7016	0.6993	2.047	2.014
3D box, $\ell=1$, RBC	61.91	57.21	0.7092	0.6927	2.259	2.363
2D full cylinder ^c	35.93	35.25	0.5734	0.5711	1.444	1.439
2D half cylinder	35.30	34.84	0.574	0.5725	1.439	1.440
2D quarter cylinder	35.31	34.87	0.574	0.5725	1.439	1.440
2D cylinder, CV ^d	17.39	17.11	0.4394	0.4377	0.993	0.995
2D cylinder, CR ^e	14.62	14.51	0.4046	0.4039	0.909	0.914
3D sphere / 2D spherical annulus ^f	15.5	16.19	0.3635	0.3374	0.796	0.744

We apply a surface Rayleigh number of $Ra=10$ and a FKA (22) viscosity contrast of $1e5$.

^a RBC stands for reflective boundary condition at the side wall with free-slip boundary.

^b PBC stands for periodic boundary conditions.

^c The sphere uses a radius ratio of 2, i.e., the core radius is half the planet radius.

^d CV means corr. volume: ratio of core area divided by mantle volume is as in 3D.

^e CR means corr. radius: ratio of core area divided by surface area is as in 3D.

^f We use a 2D spherical annulus for CHIC with 4 initial plumes; a 3D sphere was used for GAIA.

80(160 for $\ell=2$)x80 cells, for the 3D box 40x40x40 cells and for the 2D shells we use 80 shells in radial direction with 754, 377, 189, 440, 419 and 754 points per shell for the six considered cylindrical/spherical cases. Note that we compare the 2D spherical annulus of CHIC to the case of 3D sphere of GAIA.

The results obtained with CHIC are in good agreement with those obtained with GAIA, with deviations below 2% apart from the 3D box (7.6% deviation for the velocity) and the spherical annulus (7.2% deviation for the temperature), where we compare to the 3D sphere in [24], see Table II. The plots in Figure 6 show the steady-state for all cases.

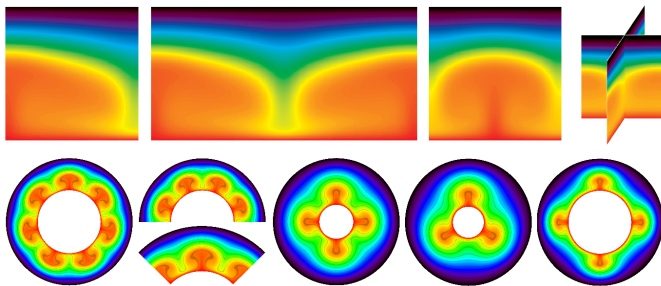


Figure 6. Convection patterns obtained with CHIC for different available geometries. See text and Table II for more details.

We do a further validation of our 2D spherical annulus implementation for isoviscous material by comparing it to the results in [13] for bottom-heated (i.e., constant bottom temperature) and internally heated convection (i.e., zero heat flux at bottom and internal heat sources), see Figure 7.

The non-dimensional radius of the core is 1.2222 and the planet radius is 2.2222. We use a resolution of 32 shells with 256 points on each shell. The CHIC results are in good agreement with the published results. The differences are less than 5%, see Table III.

The largest deviations appear for time-dependent simulations (indicated by \sim). For these cases averaged values depend

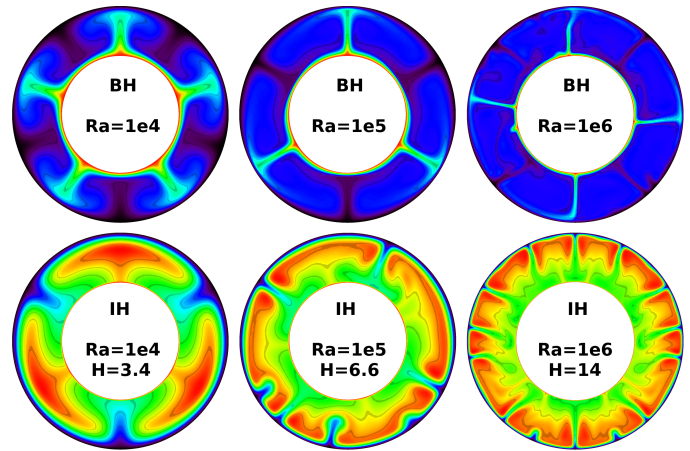


Figure 7. Temperature fields obtained for the isoviscous spherical annulus models from [13].

TABLE III. BENCHMARK COMPARISON OF CHIC (CH) TO [13] (HT)

Ra	Average RMS velocity		Nusselt number	
	CH	HT	CH	HT
1e4	38.22	37.7	4.13	4.18
1e5	157.2	~ 160	7.06	~ 7.39
1e6	~ 622	~ 640	~ 14.1	~ 14.4
Ra/H	Average RMS velocity		Average mantle temperature	
1e4 / 3.4	24.3	23.5	0.3	0.308
1e5 / 6.6	~ 76.6	~ 78.5	~ 0.36	~ 0.349
1e6 / 14	~ 252.4	~ 265	~ 0.35	~ 0.35

Isoviscous material, case 1: bottom-heated convection, case 2: internally-heated convection.

on the size of the averaging time domain (in this study an interval of up to ~ 0.2 diffusion times is applied). For this reason, typically only steady-state simulations are used in community benchmarks. Recently, an increasing attention has been drawn to benchmarks for time-dependent simulations, for example for plastic deformation and episodic overturn [26].

B. 2D compressible model

The 2D compressible implementations TALA and ALA (see Section III-D1) are compared to a benchmark published by King et al. [14]. The benchmark includes compressible simulations in a 2D Cartesian box using different dissipation numbers and Rayleigh numbers. For the comparison we apply a resolution of 80x80 cells and a dissipation number of $Di = 1$. No viscosity variation is considered. The Rayleigh number is varied between 10^4 and the maximal value that still leads to a steady-state solution.

TABLE IV. BENCHMARK COMPARISON OF CHIC (CH) TO [14] (KI)

	RMS velocity		Average temperature		Nusselt number	
	CH	KI	CH	KI	CH	KI
EBA, Ra=1e4	24.2	23.9-24.2	0.47	0.47-0.47	2.19	2.15-2.19
EBA, Ra=2e4	39.4	39.1-39.5	0.47	0.47-0.47	2.65	2.60-2.65
EBA, Ra=5e4	71.5	70.8-71.7	0.47	0.47-0.47	3.36	3.30-3.36
EBA, Ra=1e5	107.9	107.1-108.2	0.48	0.48-0.48	3.95	3.89-3.97
EBA, Ra=2e5	146.7	147.0-148.0	0.49	0.49-0.49	4.42	4.40-4.44
TALA, Ra=1e4	26.0	26.0-26.1	0.51	0.51-0.51	2.56	2.51-2.57
TALA, Ra=2e4	40.2	40.2-40.5	0.51	0.51-0.52	3.01	2.96-3.02
TALA, Ra=5e4	66.9	66.8-68.7	0.52	0.52-0.52	3.63	3.61-3.64
TALA, Ra=1e5	84.6	84.9-91.1	0.53	0.52-0.53	3.91	3.89-3.98
ALA, Ra=1e4	24.3	24.7-25.0	0.51	0.51-0.51	2.42	2.44-2.47
ALA, Ra=2e4	37.9	38.5-39.0	0.52	0.52-0.52	2.86	2.88-2.92
ALA, Ra=5e4	64.1	64.9-65.9	0.52	0.52-0.52	3.50	3.51-3.55
ALA, Ra=1e5	84.0	84.6-85.6	0.53	0.53-0.53	3.86	3.86-3.88

We validate the accuracy of the simulations by comparing the RMS velocity, the average mantle temperature and the Nusselt number in Table IV to the value range listed in [14]. CHIC compares well with the published results with deviations below two percent. Note that these small deviations appear only for some of the TALA and ALA cases, where less codes contributed to the original study, leading to a narrower value range in [14].

C. Chemical buoyancy

Density variations in the mantle occur due to temperature influences (the thermal buoyancy term in the momentum equation), chemical influences (inhomogeneous mantle due to crust subduction, local melt depletion, etc.), and compressibility effects. CHIC traces chemical density variations either via particles or with a field approach, see Section III-D3.

We compare our implementation of the chemical advection (i.e., buoyancy forces driven by chemical density variations) to the benchmark by van Keken et al. [27]. Three cases for chemical advection have been investigated in the study modelling a light layer at the bottom of a Cartesian box below a dense layer. In addition, a viscosity contrast between the two layers of 1 (case a), 10 (b) and 100 (c) is applied. The density field of all three cases is shown in Fig. 8 at a non-dimensional time of 500. For the simulations we use a spatial resolution of 200x200 grid points and 50 tracer per cell for the particle approach and a Lewis number of 10^{10} for the field approach.

The benchmark study [27] calculates the following control parameters: the growth rate of the interface at the beginning of the simulation, the maximal rms velocity and the time when the

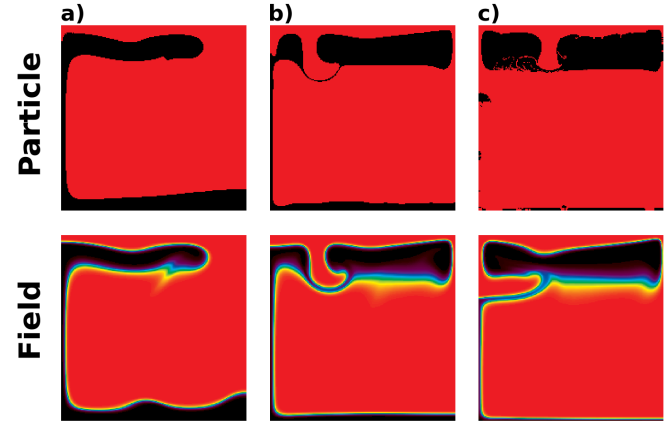


Figure 8. Chemical convection initiated by the chemical buoyancy of light material (black) below a layer of dense material (red) from benchmark [27] at non-dimensional time 500 for the particle approach (top) and the field approach (bottom).

maximal value is reached. The growth rate is calculated from the initial rms velocity increase via the following formula (we use $t=100$):

$$\Gamma = \ln(v_{rms}(t)/v_{rms}(0)) / \Delta t \quad (23)$$

Table V lists the growth rate, maximal rms velocity and time for both the particle (P) and the field (F) approach for the three cases. Our results reproduce the benchmark case almost exactly.

TABLE V. BENCHMARK COMPARISON OF CHIC (CH) TO [27] (VK)

	Growth rate Γ		Max RMS velocity		Time (Max RMS v.)	
	CH	VK	CH	VK	CH	VK
a	0.0117 (P) 0.0115 (F)	0.011- 0.0125	0.00303 (P) 0.00308 (F)	0.00289- 0.0031	213.3 (P) 208.3 (F)	206.4- 215.7
b	0.0472 (P) 0.0429 (F)	0.0392- 0.0482	0.00944 (P) 0.00917 (F)	0.00908- 0.00959	72.7 (P) 72.6 (F)	71.9- 77.1
c	0.1058 (P) 0.099 (F)	0.096- 0.1052	0.01457 (P) 0.01371 (F)	0.01385- 0.01506	50.2 (P) 49.4 (F)	48.8- 51.3

D. 1D parameterized model

To our knowledge, unlike for the mantle convection calculation, benchmark results for the 1D parameterized model have not been published. Therefore, we have validated our code by reproducing results of [8]. The results are very similar [28], but differ in detail because not all parameters used in the studies are known. The module has been integrated into the CHIC code and has been extended to include a regolith layer and compared to [29], yielding again comparable results.

We do a further validation of our 1D parameterized thermal evolution implementation by comparing it to a 2D convection calculation in a spherical annulus. The simulations are done for a Mars-like planet. We assume a Newtonian viscosity law and apply the Boussinesq approximation. The initial mantle temperature is 2000 K and the CMB temperature is 2300

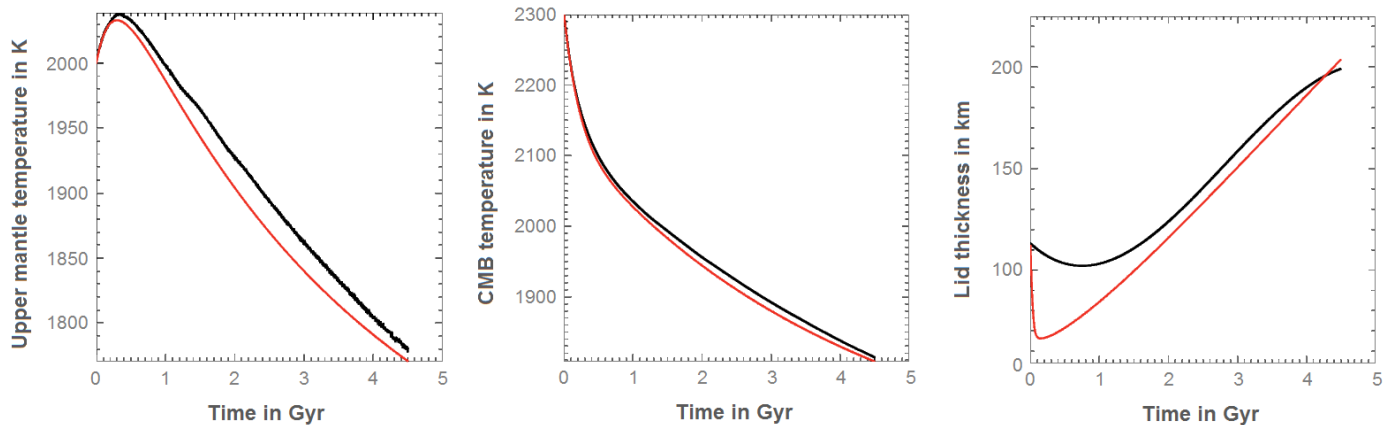


Figure 9. Upper temperature, CMB temperature and lid thickness for a thermal evolution of Mars applying either the 2D spherical annulus (black curve) or the 1D parameterized model (red).

K, the surface temperature is set to 220 K. Heat sources are homogeneously distributed in the mantle and are taken Earth-like [7]. For the 2D model, we use a quarter sphere with a radial resolution of 80 shells.

In the convection model, we define the lid over the depth where the conductive heat transport is more efficient than the convective heat transport. The lid thickness is then fitted by a third-order polynomial since the lid is strongly time-dependent and oscillations occur. The lid thickness is in the beginning larger than that of the 1D model (where we plot the total conductive layer thickness including both the lid and the upper thermal boundary layer), but shows a similar increase with time after 2 Gyr (see Figure 9). The different lid thicknesses at the beginning of the evolution can be explained by a delayed on-set of convection in the 2D model, which also leads to a slightly weaker mantle cooling at the beginning and hence a shift in the upper mantle temperature compared to the 1D model, see see Figure 9.

Our results show that the 1D parameterized model leads to a thermal evolution comparable to the results obtained with convection models.

V. CONCLUSION

We developed a new, advanced numerical code that couples different models that are needed for the investigation of habitability-relevant processes and feedback mechanisms for Earth-like or water-rich planets or moons. The code can be used with 1D and 2D/3D geometries for the silicate mantle or ice shells. The thermal state of the core, the ocean and atmosphere layer are simulated with a parameterized approach.

We have extended our earlier study [1] by a compressible formulation, which is especially of interest for planets of Earth size or larger. Chemical convection has been included to investigate buoyancy effects from density variations due to for example partial melting or subducted crust. Particles have been implemented to transport local information like the

water content through the mantle. Both OpenMP and MPI parallelisation are available to allow the usage of CHIC on standard high-performance clusters.

We have validated our implementations for the parameterized model and 2D/3D convection model by comparing CHIC to published results and by running a set of standard benchmarks. For all benchmarks, CHIC is in good agreement with literature values.

The code can be applied to investigate the possible habitability of terrestrial or water-rich planets [9] and moons, including the simulation of feedbacks between the interior and surface for stagnant-lid and plate tectonics planets.

ACKNOWLEDGMENT

L. Noack has been funded by the Interuniversity Attraction Poles Programme initiated by the Belgian Science Policy Office through the Planet Topers alliance. A. Rivoldini was supported by the PRODEX program managed by the European Space Agency in collaboration with the Belgian Federal Science Policy Office. This work results within the collaboration of the COST Action TD 1308. We thank Clemens Heistracher, Nastasia Zimov, François Labbé, and Thomas Boiveau for their contributions to the project.

REFERENCES

- [1] L. Noack, A. Rivoldini, and T. Van Hoolst, "CHIC - Coupling Habitability, Interior and Crust," INFOCOMP 2015, Brussels, Belgium, vol. ISBN: 978-1-61208-416-9, 2015, pp. 84–90.
- [2] P. van Thienen et al., "Water, life, and planetary geodynamical evolution," *Space Sci. Rev.*, vol. 129, 2007, pp. 167–203, doi: 10.1007/s11214-007-9149-7.
- [3] L. Noack and D. Breuer, "Interior and surface dynamics of terrestrial bodies and their implications for the habitability," in *Habitability on other planets and satellites: The quest for extraterrestrial life*, J.-P. de Vera and F. Seckbach, Eds. Springer, Dordrecht, 2013, pp. 203–233, doi: 10.1007/978-94-007-6546-7_12.

- [4] G. Schubert, M. N. Ross, D. J. Stevenson, and T. Spohn, "Mercurys thermal history and the generation of its magnetic field," *Mercury*, 1998, pp. 429–460, ISBN 9780816510856.
- [5] L. Noack, D. Breuer, and T. Spohn, "Coupling the atmosphere with interior dynamics: Implications for the resurfacing of venus," *Icarus*, vol. 217, 2012, pp. 484–498, doi:10.1016/j.icarus.2011.08.026.
- [6] C. Gillmann and P. Tackley, "Atmosphere/mantle coupling and feedbacks on venus," *J. Geophys. Res. Plan.*, vol. 119, 2014, pp. 1189–1217, doi:10.1002/2013JE004505.
- [7] G. Schubert, D. L. Turcotte, and P. Olson, *Mantle convection in the Earth and planets*. Cambridge University Press, Cambridge, UK, 2001, doi:10.1017/CBO9780511612879.
- [8] A. Morschhauser, M. Grott, and D. Breuer, "Crustal recycling, mantle dehydration, and the thermal evolution of Mars," *Icarus*, vol. 212, no. 2, 2011, pp. 541–558, doi:10.1016/j.icarus.2010.12.028.
- [9] L. Noack et al., "Water-rich planets: how habitable is a water layer deeper than on Earth?" *Icarus*, in press, doi:10.1016/j.icarus.2016.05.009.
- [10] L. Stixrude and C. Lithgow-Bertelloni, "Thermodynamics of mantle minerals–i. physical properties," *Geophys. J. Int.*, vol. 162, no. 2, 2005, pp. 610–632, doi:10.1111/j.1365-246X.2005.02642.x.
- [11] J. Bouchet, S. Mazevet, G. Morard, F. Guyot, and R. Musella, "Ab initio equation of state of iron up to 1500 GPa," *Physical Review B*, vol. 87, no. 094102, 2013, pp. 1–8, doi:10.1103/PhysRevB.87.094102.
- [12] D. J. Stevenson, T. Spohn, and G. Schubert, "Magnetism and thermal evolution of the terrestrial planets," *Icarus*, vol. 54, 1983, pp. 466–489, doi:10.1016/0019-1035(83)90241-5.
- [13] J. W. Hernlund and P. J. Tackley, "Modeling mantle convection in the spherical annulus," *Physics of the Earth and Planetary Interiors*, vol. 171, no. 1, 2008, pp. 48–54, doi:10.1016/j.pepi.2008.07.037.
- [14] S. D. King et al., "A community benchmark for 2-d cartesian compressible convection in the earth's mantle," *Geophys. J. Int.*, vol. 180, no. 1, 2010, pp. 73–87, doi:10.1111/j.1365-246X.2009.04413.x.
- [15] U. R. Christensen, "Convection with pressure- and temperature-dependent non-newtonian rheology," *Geophys. J. R. astr. Soc.*, vol. 77, 1984, pp. 343–384, doi:10.1111/j.1365-246X.1984.tb01939.x.
- [16] S. Zhong, D. A. Yuen, and L. N. Moresi, "Numerical methods in mantle convection," *Treatise on Geophysics*, vol. 7, 2007, pp. 227–252, doi:10.1016/B978-044452748-6.00118-8.
- [17] S. V. Patanker, "A calculation procedure for two-dimensional elliptic situations," *Numerical Heat Transfer V*, 1981, pp. 409–425, doi:10.1080/01495728108961801.
- [18] O. Schenk and K. Gärtner, "On fast factorization pivoting methods for symmetric indefinite systems," *Elec. Trans. Numer. Anal.*, vol. 23, 2006, pp. 158–179, ISSN 1068-9613.
- [19] S. Karato and P. Wu, "Rheology of the upper mantle: A synthesis," *Science*, vol. 260, 1993, pp. 771–778, doi:10.1126/science.260.5109.771.
- [20] G. Hirth and D. Kohlstedt, "Rheology of the upper mantle and the mantle wedge: A view from the experimentalists," *Inside the subduction Factory*, 2003, pp. 83–105, doi:10.1029/138GM06.
- [21] R. Katz, M. Spiegelman, and C. Langmuir, "A new parameterization of hydrous mantle melting," *Geochem. Geophys. Geosyst.*, vol. 4, no. 9 – 1073, 2003, pp. 1–19, doi:10.1029/2002GC000433.
- [22] L. Noack and D. Breuer, "First- and second-order Frank-Kamenetskii approximation applied to temperature-, pressure- and stress-dependent rheology," *Geophys. J. Int.*, vol. 195, 2013, pp. 27–46, doi:10.1093/gji/ggt248.
- [23] B. Blankenbach et al., "A benchmark comparison for mantle convection codes," *Geophys. J. Int.*, vol. 98, 1989, pp. 23–38, doi:10.1111/j.1365-246X.1989.tb05511.x.
- [24] L. Noack and N. Tosi, "High-performance modelling in geodynamics," in *Integrated Information and Computing Systems for Natural, Spatial, and Social Sciences*, C.-P. Rückemann, Ed. IGI Global, 2013, pp. 324–352, doi:10.4018/978-1-4666-2190-9.ch016.
- [25] C. Hüttig and K. Stemmer, "Finite volume discretization for dynamic viscosities on voronoi grids," *Physics of the Earth and Planetary Interiors*, vol. 171, 2008, pp. 137–146, doi:10.1016/j.pepi.2008.07.007.
- [26] N. Tosi et al., "A community benchmark for viscoplastic thermal convection in a 2-d square box," *Geochem. Geophys. Geosyst.*, vol. 16, 2015, pp. 2175–2196, doi:10.1002/2015GC005807.
- [27] P. E. van Keken et al., "A comparison of methods for the modeling of thermochemical convection," *J. Geophys. Res.: Solid Earth*, vol. 102, no. B10, 1997, pp. 22477–22495, doi:10.1029/97JB01353.
- [28] T. Boiveau, "Convection mantellique dans les plantes telluriques," *Rapport de stage*, unpublished.
- [29] N. Tosi, M. Grott, A.-C. Plesa, and D. Breuer, "Thermochemical evolution of mercurys interior," *J. Geophys. Res. Plan.*, vol. 118, 2013, pp. 1–14, doi:10.1002/jgre.20168.